Correlations among the optical properties of cirrus-cloud particles: Microphysical interpretation

J. Reichardt,[1,2] S. Reichardt,[1,2] M. Hess,[3] and T. J. McGee[2]

Abstract. Cirrus measurements obtained with a ground-based polarization Raman lidar at 67.9°N in January 1997 reveal a strong positive correlation between the particle optical properties, specifically depolarization ratio $\delta_{\rm par}$ and extinction-to-backscatter (lidar) ratio S, for $\delta_{\rm par} <\sim 40\%$, and an anti-correlation for $\delta_{\rm par} >\sim 40\%$. Over the length of the measurements the particle properties vary systematically. Initially, $\delta_{\rm par} \approx 60\%$ and $S \approx 10\,{\rm sr}$ are observed. Then, with decreasing $\delta_{\rm par}$, S first increases to $\sim 27\,{\rm sr}$ ($\delta_{\rm par} \approx 40\%$) before decreasing to values around 10 sr again ($\delta_{\rm par} \approx 20\%$). The analysis of lidar humidity and radiosonde temperature data shows that the measured optical properties stem from scattering by dry solid ice particles, while scattering by supercooled droplets, or by wetted or subliming ice particles can be excluded. For the microphysical interpretation of the lidar measurements, ray-tracing computations of particle scattering properties have been used. The comparison with the theoretical data suggests that the observed cirrus data can be interpreted in terms of size, shape, and, under the assumption that the lidar measurements of consecutive cloud segments can be mapped on the temporal development of a single cloud parcel moving along its trajectory, growth of the cirrus particles: Near the cloud top in the early stage of cirrus development, light scattering by nearly isometric particles that have the optical characteristics of hexagonal columns (short, column-like particles) is dominant. Over time the ice particles grow, and as the cloud base height extends to lower altitudes characterized by warmer temperatures they become morphologically diverse. For large S and depolarization values of $\sim$ 40%, the scattering contributions of column- and plate-like particles are roughly the same. In the lower ranges of the cirrus clouds, light scattering is predominantly by plate-like ice particles. This interpretation assumes random orientation of the cirrus particles. Simulations with a simple model suggest, however, that the positive correlation between S and $\delta_{\rm par}$, which is observed for depolarization ratios $<$ 40% mainly at low cloud altitudes, can be alternatively explained by horizontal alignment of a fraction of the cirrus particle population.

1. Introduction

The microphysics of aerosols and clouds affect atmospheric processes of all scales [*Baker*, 1997]. The retrieval of microphysical information from remotely sensed optical data such as those acquired with lidar is therefore a worthwhile research effort. If the sizes of the scattering particles are comparable to the wavelength of the radiation used for the observation, one can exploit the wavelength dependence of the cloud optical properties to gain insight into the microphysics of the particulate scatterers. Over the years, sophisticated lidar instrumentation and retrieval algorithms have been developed for this purpose that have been successfully applied to stratospheric aerosols [*Del Guasta et al.*, 1994; *Wandinger et al.*, 1995], polar stratospheric clouds [*Carslaw et al.*, 1998; *Mehrtens et al.*, 1999], tropospheric aerosols [*Müller et al.*, 1998; *Müller et al.*, 2001], and contrails [*Sassen et al.*, 2001].

However, these techniques are generally not applicable to tropospheric or stratospheric clouds with populations of particles that are predominantly much larger than the optical observation wavelengths. For these clouds, other methods are required for the retrieval of microphysical information. Multi-instrument techniques, such as the approach based on combined lidar and radar measurements [*Intrieri et al.*, 1993], have been proposed, but, since instrument clusters are not always available, it seems desirable to attempt extraction of microphysical data from lidar measurements alone.

For cirrus clouds, which are the focus of this work, remote measurements of particle depolarization ratio $\delta_{\rm par}$ have proven to be highly valuable for studies of ice-cloud microphysics, dynamics, and optical displays (see, e.g., *Sassen* [1991], *Sassen* [1992], *Sassen and Takano* [2000], *Sassen and Benson* [2001], *Sassen et al.* [2001]). The success of using depolarization ratio for the interpretation of cirrus data stems from the fact that $\delta_{\rm par}$ is one of the two cloud optical properties accessible to lidar that do not depend on the particle number density. Thus, $\delta_{\rm par}$ contains (particle population-averaged) information about particle morphology. To distinguish $\delta_{\rm par}$ from cloud optical properties that do depend

[1]Joint Center for Earth Systems Technology, University of Maryland Baltimore County, Baltimore, Maryland, USA.

[2]Atmospheric Chemistry and Dynamics Branch, Laboratory for Atmospheres, NASA Goddard Space Flight Center, Greenbelt, Maryland, USA.

[3]Remote Sensing Technology Institute, DLR - German Aerospace Center, Oberpfaffenhofen, Weßling, Germany

Paper number .
0148-0227/02/$9.00

on number density (such as extinction and backscatter coefficient), we use the term particle optical property.

The second particle optical property that can be measured with lidar is the extinction-to-backscatter (lidar) ratio S, and it appears promising to include S in the microphysical analysis of cirrus measurements. To our knowledge, only two cirrus studies based on lidar ratio and depolarization ratio have been published so far. *Del Guasta* [2001] retrieved cloud-averaged lidar ratios for Antarctic cirrus clouds from their measurements taken with an elastic polarization lidar, and interpreted the optical data in terms of ice crystal shape. *Eloranta et al.* [2001] investigated correlations among particle lidar and depolarization ratios of cirrus clouds measured over the continental United States with their polarization high spectral resolution lidar [*Eloranta and Piironen*, 1997], and compared experimental and theoretical values of lidar ratio.

Recently, *Reichardt et al.* [2002b] have reported on the correlation between depolarization and lidar ratio found in Arctic and mid-latitude cirrus clouds, and discussed the implications of their findings for spaceborne remote sensing. In this follow-up article, we give a microphysical interpretation of these measurements. Since for the microphysical analysis it is instructive to look at the temporal evolution of the particle optical properties of the cirrus clouds, we thus restrict our discussion to the long-duration cirrus observations made with the GKSS Raman lidar [*Reichardt et al.*, 1996] above the Swedish research facility Esrange (67.9 °N, 21.1 °E) in January 1997.

2. Observations

Figures 1–3 show three long-duration observations of cirrus clouds made over Esrange in January 1997. These measurement cases have been chosen for outstanding data quality; for a time-height visualization of the cirrus observations and a detailed description of the data evaluation process see *Reichardt et al.* [2002b]. For each lidar observation, three measurement intervals have been selected to study the development of the clouds over time. All cirrus clouds are optically thin, as can be seen from the particle and molecular backscatter coefficients. Generally, the particle backscatter coefficient exhibits a much larger variability with height than the particle depolarization ratio or the lidar ratio, indicating that the particle number density rather than the particle optical properties, and hence the microphysical properties, changes rapidly within the clouds.

In Fig. 4 the temporal evolution of the relation between the particle optical properties, specifically the particle depolarization ratio and lidar ratio, is illustrated. The experimental results can be summarized as follows. Firstly, for each measurement interval, at least one of the correlation patterns emerges that are evident in the combined data set of the three observation nights (Fig. 5). Secondly, during each cirrus event, the particle properties exhibit the same systematic variation over the length of each measurement (3–7.5 hours). Initially, $\delta_{\mathrm{par}} \approx 60\%$ and $S \approx 10\,\mathrm{sr}$ are observed. Then, with decreasing δ_{par}, S first increases to $\sim 27\,\mathrm{sr}$ ($\delta_{\mathrm{par}} \approx 40\%$) before decreasing to values around 10 sr again ($\delta_{\mathrm{par}} \approx 20\%$).

Our data have been measured at a wavelength of 355 nm. Cirrus observations with the same instrument over northern Germany have yielded similar ranges of S and δ_{par} values, except that $\delta_{\mathrm{par}} > 35\%$ is rarely measured [*Reichardt*, 1999]. In contrast, if compared to other lidar data sets that have been used for the retrieval of cirrus microphysics, some remarkable discrepancies can be found. *Sassen and Comstock* [2001] retrieved cloud-averaged lidar ratios at 694 nm for various categories of cirrus clouds observed over central North America. These lidar ratios tend to be larger than those shown in Figs. 1–4, the S distributions peak at 30 sr, and are weighted more heavily to larger S values. Likewise, *Del Guasta et al.* [1993] reported a considerable number of Antarctic cirrus cloud observations with cloud-averaged $S > 30\,\mathrm{sr}$ for $T_{\mathrm{C}} < -30\,^{\circ}\mathrm{C}$ (observation wavelength of 532 nm). Direct measurements of lidar-ratio profiles at 532 nm by *Eloranta et al.* [2001] yielded a distribution of S occurrences with greater similarity to our measurements (most of the data between 10 and 30 sr), but the center of the distribution appears to be at slightly larger S values than at 355 nm, and S data $> 30\,\mathrm{sr}$ are observed (central North America site). On the other hand, particle depolarization ratios of *Sassen et al.* [2000] (δ_{par} between 35% and 60% for $T_{\mathrm{C}} < -25\,^{\circ}\mathrm{C}$; tropical western Pacific Ocean; measurement wavelength of 1064 nm), *Sassen and Benson* [2001] ($> 30\%$ for $T_{\mathrm{C}} < -30\,^{\circ}\mathrm{C}$) and of *Eloranta et al.* [2001] (most $\delta_{\mathrm{par}} > 30\%$) agree well with our observations, while the depolarization data of *Del Guasta et al.* [1993] are significantly smaller with values predominantly $< 22\%$. The discrepancies between the cirrus optical data sets mentioned may be due to the different geographical locations at which the cirrus clouds were observed, and, in the case of lidar ratio,

Figure 1. Particle backscatter coefficient (β), particle depolarization ratio (δ_{par}), and lidar ratio (S) for a cirrus system evolving over time. The measurement was taken over Esrange, Sweden, on 8 January 1997. Of the long-duration observation three measurement periods are shown (times corresponding to the centers of the intervals are indicated). Measurement wavelength is 355 nm. Error bars indicate the standard deviation due to signal noise. Molecular backscatter coefficients (dashed curves) are given for comparison.

Figure 2. Same as in Fig. 1, but for 16 January 1997.

Figure 3. Same as in Fig. 1, but for 19 January 1997.

to the differing direct or indirect retrieval techniques. Differences in measurement wavelength might play a role also, although a wavelength effect would not be expected unless significant numbers of very small ice particles are present in the cirrus clouds. In view of this data review, it would be interesting to compare our observations with measurements obtained with other UV polarization Raman lidars at different locations. To our knowledge, however, no 355-nm data are available at this time. To address the issues discussed above, simultaneous measurements of depolarization and lidar ratio at ultraviolet and visible wavelengths should be performed in the future.

Figure 5 concisely summarizes the results of the correlation studies and the analysis of cirrus temperature associated with the particle optical properties which have been discussed by *Reichardt et al.* [2002b], and which are important for the microphysical interpretation proposed here. The combined data show two distinct linear correlation patterns. δ_{par} and S are negatively correlated when the depolarization ratio is high, and they are positively correlated when the depolarization ratio is low. Furthermore, the particle optical properties depend on the ambient cloud temperature T_{C}. The coldest T_{C} values are found for high δ_{par} and low S, warmest T_{C} values for low δ_{par} and low S. For large S, where the low- and high-δ_{par} data subsets merge, T_{C} lies approximately in the middle of the observed temperature range. Interestingly, this temperature is roughly the same as the mid-cloud temperature at which *Platt and Dilley* [1981] noted a change in their cirrus backscatter-to-extinction ratio data, a change they attributed to a transition in particle morphology.

The correlations among S and δ_{par}, and their dependence on T_{C} suggest that the observations can be interpreted in terms of the shape and size of the scattering cirrus particles (scatterers of any shape formed from frozen water) for two reasons. Firstly, lidar-relevant particle optical properties are determined by the phase matrix elements at 180-degree scattering angle of light scattering by the cirrus particle population, which in turn depend on the morphology of the cloud particles. Secondly, T_{C} is the principal factor that controls basic crystal shape [*Mason et al.*, 1963]. Before we investigate this hypothesis, we first discuss the ray-tracing calculations we have performed in order to derive theoretical particle optical properties for comparison with the observations.

3. Ray-tracing Calculations

Atmospheric crystals rarely have perfect shape, but exhibit distortions such as ice core inhomogeneities and angles between crystal faces that deviate from the theoretical values. While particle depolarization ratios calculated with the ray-tracing technique often match values observed in cirrus clouds regardless of the assumed imperfections, theoretical lidar ratios are very sensitive to the assumptions made and can be wrong by orders of magnitude. In order to derive realistic theoretical optical data, we account for crystal irregularities in our ray-tracing calculations by statistical roughening of the crystal surfaces [*Hess et al.*, 1998]. The crystals have principally hexagonal shape and are random in orientation, surface roughness is assumed to be the same for columns or plates of all aspect ratios. To reduce statistical errors of the computations, scattering phase matrix elements calculated at 179- and 180-degree scattering angle are averaged. Model runs are performed for different surface roughnesses, and values of this parameter are selected for which the calculated δ_{par} and S values both fall within the observation ranges of these quantities. Figure 6 shows

Figure 5. Combined particle depolarization ratio versus lidar ratio scatter plot of the cirrus measurements shown in Figs. 1–3. The distribution of the data points is bifurcated. The domains chosen for splitting the data set into two subsets of data points with high δ_{par} and low δ_{par} are indicated by differently slanted lines. Within each group, data are strongly correlated. Corresponding regression lines are shown. Cloud temperatures that are associated with the particle optical properties of each data subset are indicated for lidar ratios of 12 and 25 sr (cf. *Reichardt et al.* [2002b]).

Figure 4. Particle depolarization ratio versus lidar ratio scatter plots of the cirrus measurements on 8 (top), 16 (center), and 19 (bottom) January 1997 shown in Figs. 1–3.

Figure 6. Particle depolarization ratio versus lidar ratio scatter plot of solid hexagons with aspect ratios between 0.04 and 0.3 (plates; Δ, $\blacktriangle$), and aspect ratios between 1.3 and 5.9 (columns; ∇, $\blacktriangledown$). The data have been derived with ray-tracing calculations. Assumed surface roughness of the artificial crystals is indicated, filling of symbols alternates with surface roughness. The display range of the cirrus observations is shown for comparison (dotted rectangle).

the results of calculations for hexagons with 0%, 1%, and 10% surface roughness. Generally, an increase in surface roughness leads to higher S and lower δ_{par}. For the comparison with our observations, we choose data obtained with 0% (plates) and 1% (columns) surface roughness.

One shortcoming of the ray-tracing approach is that physical-optics effects are not taken into account. Furthermore, numerical instability is a problem in the direct backward-scattering direction, so ray-tracing data have to be used with caution if lidar measurements are to be interpreted. For crystals with imperfections, however, the ray-tracing technique may still be applicable, because crystal shape distortions tend to smooth the features of the scattering phase matrix elements at lateral and backward scattering angles.

4. Microphysical Interpretation

Figure 7 shows the domains of the observed particle optical data along with the results of the ray-tracing calculations. Depolarization ratios of relatively isometric crystals

Figure 7. Theoretical optical data of plates (▲) and columns (▼), and domains and regression lines of the high-δ_{par} and low-δ_{par} data subsets. Aspect ratios of plates decrease, aspect ratios of columns increase with lidar ratio.

match the values of the high-δ (cold T_C) and low-δ (warm T_C) data subsets for small S. For larger S, the computed optical properties of elongated columns and thin plates mark the boundaries of the measurements. This implies that for large S the observed cirrus clouds have the optical properties of mixtures of columnar and planar particles. Since in natural ice clouds length and aspect ratio (length divided by width) of the ice crystals are correlated (small crystals tend to have aspect ratios close to one, whereas large columns and plates have aspect ratios $\gg 1$ and $\ll 1$, respectively [*Auer and Veal*, 1970]), the optical data indicates an increase in size of the scattering cirrus crystals with S.

Despite the good agreement between theoretical and observed optical properties, however, the translation of the optical properties into actual shapes and sizes of the cirrus particles is not straight forward. It is complicated by the fact that cirrus clouds usually contain particles of various sizes and shapes, and that the relation between microphysical and optical properties is not unique. E.g., hexagonal plates and hollow columns, bullet rosettes, and aggregates have almost the same scattering characteristics, if rough crystal surfaces are assumed [*Yang and Liou*, 1998]. For this reason, it would be more accurate to say that plate-*like* or column-*like* particles dominated cirrus scattering when the optical signature of hexagonal plates or columns was observed. Furthermore, composite particles have been shown to scatter similarly to the ensemble of basic crystals that formed it [*Macke*, 1993; *Yang and Liou*, 1998]. So a small ice particle consisting of one or more relatively large ice crystals may still have a higher S value than a large ice particle formed from relatively small crystals. With these limitations in mind, we propose the following microphysical interpretation of the observations. In the coldest regions of the clouds, approximately isometric ice particles form. For increasing T_C, the ice particles get larger and consist of a mixture of column-like and plate-like scatterers, but remain predominantly column-like. Around $T_C = -50°C$, the dominant characteristics of the particles gradually shifts from column- to plate-like. At even warmer temperatures in the lower regions of the cirrus clouds, size and morphological complexity of the plate-like particles increase with T_C. This interpretation combines in a consistent manner the observed cirrus optical properties and temperature data with theoretical studies on light scattering by atmospheric ice particles [*Macke*, 1993; *Hess et al.*, 1998; *Yang and Liou*, 1998], laboratory experiments on the formation and growth of ice crystals [*Heymsfield*, 1973; *Gonda and Yamazaki*, 1978], and *in situ* particle sampling [*Heymsfield*, 1973]. According to the proposed scenario, the ice clouds observed over Esrange would have had a vertical habit distribution that followed the common, yet not general, pattern of small, sphere-like crystals near the cloud top, relatively large mono-crystals of imperfect hexagonal symmetry or simple bullet rosettes around the center of the ice cloud, and crystal clusters of arbitrary over-all shape in the lower cirrus ranges (see *Heymsfield and Iaquinta* [2000] and *Yang et al.* [2001] for good examples of height-dependent habit variations in cold cirrus clouds).

It is important to note that this microphysical interpretation does not draw upon the observed evolution of the optical properties over time, as shown in Fig. 4. It is a static interpretation in the sense that for each of the three cirrus cases considered all observation intervals are treated as if independent of one another. This assumption led to the time-independent presentation of the experimental data in Fig. 5, and to the interpretation given above. However, Fig. 4 strongly suggests that the systematic change in particle optical properties from one measurement interval to the other may be interpreted in terms of growth; or more generally morphological development of the cirrus particles. The difficulty with this dynamical interpretation of the lidar data is that one has to assume that the lidar observations of consecutive cloud segments can be mapped on the temporal development of a single cloud parcel moving along its trajectory. This requires the cloud layer, though varying in vertical structure and particle number density, to be composed of similar particles throughout its horizontal range at any given time over the observation period. Because of the generally high variability of the atmosphere, it cannot be expected that this condition is often met, and therefore the dynamical interpretation is a more speculative one than the static interpretation at this point. However, at least in one measurement case, initial results obtained with a coupled microphysical and optical model currently being developed are consistent with the hypothesis of particle growth [*Reichardt et al.*, 2002a].

5. Discussion

The interpretation given above is plausible. However, since extraction of microphysical information from optical remote measurements is an ill-posed problem, and since atmospheric ice particles can have diverse morphology, alternative explanations are conceivable. E.g., the decrease in particle depolarization ratio with S observed in the high-δ_{par} data subset may not be due to an increasing fraction of plate-like particles. Instead it may be the effect of column basal faces hollowing out during growth, since hollow columns have lower δ_{par} values than solid specimen [*Takano and Liou*, 1995]. We have tried to avoid this morphological problem by referring to the cirrus particles as column- or plate-like particles rather than columns or plates. We may be able to refine our microphysical interpretation when reliable theoretical optical data for ice particles other than columns and plates become available to us. Here, except for

shape, we discuss the other underlying fundamental assumptions of our microphysical interpretation. Specifically, these assumptions are that the cirrus particles consist of frozen water and are in random orientation, and that sublimation does not play a role.

5.1. Cirrus Particle Phase

Because of the very cold cloud temperatures (below $-40°$C) for the overwhelming majority of the cirrus data), it is a justified assumption that scattering is by dry solid ice particles only. At these temperatures, noticeable effects are highly unlikely that stem from quasi-liquid layers on the crystals [*Wettlaufer*, 1999] or that are due to co-existing liquid droplets. To our knowledge, the coldest temperatures at which liquid droplets have been reported to exist in cirrus and convective clouds are $-36°$C and $-37.5°$C, respectively [*Sassen et al.*, 1985; *Rosenfeld and Woodley*, 2000]. Liquid droplets of aqueous acids can exist at even colder atmospheric temperatures. Freezing point depression resulting from an influx of stratospheric volcanic aerosols into the cirrus-generating regions has been used to explain the observation of short-lived cloud cells of liquid drops in cirrus clouds at $-49°$C [*Sassen*, 1992]. However, this rare phenomenon can be excluded from the discussion here, because at the time of the measurements the aerosol content of the lower stratosphere was very low.

5.2. Random Orientation

The microphysical interpretation given in Sect. 4 is based on the assumption that at all measurement times the cirrus particles were randomly oriented in three dimensions (3D-orientation). As a consequence, we had to invoke an increase in morphological complexity of plate-like particles in order to explain the low S values in the lower cirrus layers.

An alternative mechanism that could explain more elegantly the low-$\delta_{\rm par}$ data subset, as well as (if the dynamical interpretation is considered) the transition between the two groups of correlated data, is the departure of an increasing fraction of the particle population from a random orientation as one approaches the cloud base. Falling ice particles larger than a critical size ($>$ 100–200 μm, depending on shape [*Sassen*, 1980]) have the tendency to assume an orientation with their maximum geometrical dimension in the horizontal plane (2D-orientation). If crystal faces of these 2D-oriented ice particles are (almost) perfectly aligned horizontally, the lidar signature shows extremely low $\delta_{\rm par}$ and S values due to specular reflections of laser light into the lidar receiver. However, it is relatively unlikely that 2D-oriented columnar particles are aligned in this peculiar manner, since they can rotate about their horizontally oriented long axis easily. This is the reason why the optical display associated with this special orientation of hexagonal columns, the Parry arc, is rarely observed [*Sassen and Takano*, 2000]. As a consequence, horizontal alignment of columns remains generally undetected by lidar. Contrarily to the prism faces of aligned columns, horizontal orientation of the basal crystal faces of 2D-oriented plates is better preserved, even though they may fall with a swaying motion. Therefore it is generally accepted that observed very low depolarization ratios [*Platt et al.*, 1978] and lidar ratios [*Ansmann et al.*, 1992] are generated by 2D-oriented planar particles [*Platt*, 1978; *Sassen*, 1980; *Sassen and Benson*, 2001].

In the following, we show that the assumption of 2D-oriented ice particles being present is consistent with the linear correlation between S and $\delta_{\rm par}$ observed in the low-$\delta_{\rm par}$ cirrus data. In our simple model, we assume that the simulated cirrus cloud consists of a population of identical ice particles, of which a fraction a is in perfect 2D-orientation while the other particles remain randomly oriented. Then the cloud optical properties as a function of a are given by

$$S(a) = \frac{1 + a(R_{\rm G} - 1)}{1 + a(R_{\rm G} R_{\rm S}^{-1} - 1)} S^{\rm 3D} ,$$

$$\delta_{\rm par}(a) = \frac{1 + a\{R_\delta[(1 + \delta_{\rm par}^{\rm 3D})/(1 + \delta_{\rm par}^{\rm 2D})] R_{\rm G} R_{\rm S}^{-1} - 1\}}{1 + a\{[(1 + \delta_{\rm par}^{\rm 3D})/(1 + \delta_{\rm par}^{\rm 2D})] R_{\rm G} R_{\rm S}^{-1} - 1\}} \delta_{\rm par}^{\rm 3D},$$

where $R_{\rm G} = G^{\rm 2D}/G^{\rm 3D}$, $R_{\rm S} = S^{\rm 2D}/S^{\rm 3D}$, and $R_\delta = \delta_{\rm par}^{\rm 2D}/\delta_{\rm par}^{\rm 3D}$ are the ratios of geometrical cross section G, lidar ratio, and depolarization ratio, respectively, for 2D-oriented cirrus particles with respect to the randomly oriented 3D case. For large thin plates, we have $R_{\rm G} \approx 2$. This means that on horizontal orientation, G of the particles, and hence the ex-

Figure 8. Profiles of particle backscatter coefficient, particle depolarization ratio, and lidar ratio for the cirrus cloud measured over Geesthacht, Germany, around 17:23 UT on 27 November 1995 (top row). Values of β below 7 km have been multiplied by 0.33 to fit into the display range. Particle depolarization ratio versus lidar ratio scatter plot of this measurement, and calculated optical data of a hypothetical cirrus cloud consisting of randomly oriented (S = 29.5 sr, $\delta_{\rm par}$ = 40%) and horizontally aligned (S = 2 sr, $\delta_{\rm par}$ = 2%) ice particles (thick solid curve) (bottom). Numbers indicate fraction of aligned particles. Display range of the cirrus observations over Esrange, and data-subset domains and regression lines are shown for comparison.
The measurement on 27 November 1995 is one of the rare cirrus cases for which reliable height-resolved profiles of lidar and depolarization ratio could be obtained over Geesthacht (because measurement conditions were generally not favorable). $\delta_{\rm par}$ and S are correlated; for $S > 8$ sr, data points fall into the Esrange low-depolarization domain. Predominantly, these data points come from the cloud layer above 8 km.

tinction coefficient, increase by this relatively small factor. On the other hand, the extinction-to-backscatter (lidar) ratios of 2D-oriented particles are 5–10 times smaller than those of randomly oriented scatterers. Apparently, even in cirrus clouds with small fractions of 2D-oriented particles, cloud backscattering is strongly affected by the specular reflections of the aligned particles, while cloud extinction is still determined by the entire particle population.

In order to calculate $S(a)$ and $\delta_{\rm par}(a)$, we need to know reliable values for lidar and depolarization ratios of cirrus particles in 2D- and 3D-orientation. Optical modeling can provide $S^{\rm 3D}$ and $\delta^{\rm 3D}_{\rm par}$, however, due to methodological limitations, calculations for 2D-oriented particles are currently not available. For this reason, we use instead as input to our calculations experimental particle optical data that can be clearly attributed to light scattering by ice particles in either random or horizontal orientation. For 3D-oriented particles we assume $S^{\rm 3D} = 29.5\,{\rm sr}$ and $\delta^{\rm 3D}_{\rm par} = 40\%$, which are approximately the optical properties of particles in the low-$\delta_{\rm par}$ data group for large S.

Values for $S^{\rm 2D}$ and $\delta^{\rm 2D}_{\rm par}$ are taken from cirrus data acquired on 27 January 1995 over Geesthacht, Germany, with the same lidar instrument that was deployed in Esrange. Cloud profiles of backscatter coefficient, particle depolarization ratio, and lidar ratio are shown in Fig. 8. On this day, two layers of ice clouds were observed. In the lower layer, $\delta_{\rm par}$ and S decreased gradually from the cloud base to the height of the backscatter maximum, and increased subsequently to the cloud-layer top. $\delta_{\rm par}$ and S at the boundaries of the lower cloud layer are similar to those found in the upper cloud layer. This optical signature is certainly the result of horizontal particle orientation, and we choose the minimum values of lidar and depolarization ratio, i. e., 2 sr and 2%, respectively, for $S^{\rm 2D}$ and $\delta^{\rm 2D}_{\rm par}$ in our simulations.

The model results are presented in Fig. 8, along with the domains of the Esrange data subsets. As expected, alignment of a relatively small fraction of cirrus particles leads to a substantial reduction in S and $\delta_{\rm par}$. The synthetic depolarization ratio exhibits a dependence on lidar ratio that is similar to the measured correlation. Considering the simplicity of the model, it is not surprising that simulated and observed $\delta_{\rm par}$-versus-S data do not match exactly. With $\delta^{\rm 2D}_{\rm par} \approx 10\%$, it is possible to achieve close agreement between model and measurement, but sensitivity studies show that the theoretical relation only slightly deviates from the one shown, if $S^{\rm 2D}$ and $\delta^{\rm 2D}_{\rm par}$ are varied within limits that are reasonable for aligned planar cirrus particles ($\sim$ 2–5 sr, $\sim$ 2–5%). This study supports the idea that horizontal particle alignment is the main cause for the relation between S and $\delta_{\rm par}$ in the low-depolarization domain of the Esrange data. However, as detailed below, there are arguments against this interpretation.

If orientation of the cirrus particles occurred during our measurements over Esrange, why then did we never detect extremely low lidar and depolarization ratios such as those observed in the lower cirrus layer of the Geesthacht measurement? One explanation could be that the GKSS Raman lidar was not sensitive to light scattering by horizontally aligned cirrus particles at that time. This mobile lidar system was transported to Esrange in December 1996, and was setup for its deployment under difficult winter conditions. So it is perfectly possible that the instrument was pointing a couple of degrees off zenith. In this case, as shown by *Sassen and Benson* [2001], the influence of 2D-oriented ice particles on the lidar measurements would have been greatly reduced, if not annihilated, and the Esrange data discussed here would have the optical signature of (quasi) randomly oriented scatterers. Another reason for the absence of $S < 8\,{\rm sr}$ and $\delta_{\rm par} < 15\%$ in the Esrange data could be that the oriented particles sensed by the lidar were in themselves disordered aggregations of crystals. To our knowledge, scattering signatures of these particles have not been calculated, but it can be speculated that the optical properties of these particles, if aligned in the horizontal plane, would be similar to those of the randomly arrayed ensemble of constituting crystals, thus covering up their reduced orientational freedom [*Sassen*, 1980]. If this were true, we would have to infer that the 2D-oriented cirrus particles which produced the optical display of extreme particle properties over northern Germany had a simpler morphology than those observed above Esrange. In view of the growth conditions at Esrange (from lidar humidity and radiosonde temperature data the diffusional mass growth rate [*Pruppacher and Klett*, 1980] can be estimated to be at least a factor of two higher over Geesthacht than over Esrange), this appears to be rather unlikely.

Figure 9. Profiles of particle backscatter coefficient, particle depolarization ratio, and lidar ratio for the cirrus cloud measured over Esrange, Sweden, around 05:04 UT on 15 January 1997 (top row), and particle depolarization ratio versus lidar ratio scatter plot of this measurement (bottom row). Theoretical optical data, data-subset domains and regression lines are shown for comparison.

With regard to the issue of particle orientation, the discussion of the cirrus measurement taken on 15 January 1997 over Esrange is instructive (Fig. 9). On this day, depolarization ratios decreased with height without much variation, with $\delta_{\rm par}$ values between 24% at the base and 16% at the top of the cloud. The observation of high values of S (20–27 sr) makes it impossible to explain these rather low depolarization ratios in terms of particle horizontal alignment. Instead,

the agreement between measured and theoretical data suggests that the ice cloud on 15 January 1997 consisted of large plate-like particles in 3D-orientation. This cirrus measurement supports the underlying assumption about orientational randomness that is made for the microphysical interpretation put forward in Section 4. However, it also shows that not in all measurement cases the optical properties of cirrus clouds with large lidar ratios carry the signature of mixtures of plate-like and column-like ice particles (on 15 January 1997, δ_{par} and S were correlated, but column-like scatterers were apparently absent).

In summary, the correlation between lidar and depolarization ratio found for δ_{par} <40% may be viewed as the result of horizontal alignment of planar ice particles, or may be attributed to the presence of randomly oriented plate-like scatterers. Since good arguments exist for the two positions (or for a combination of both), more studies are required to shed some light on the mechanisms that lead to this optical phenomenon.

5.3. Sublimation

It might be argued that sublimation led to the observed decrease in depolarization ratio for warmer temperatures and lower cloud altitudes. Experimental studies show that evaporating ice crystals acquire rounded shapes with smooth surfaces [*Nelson*, 1998], and it appears obvious to conclude that these increasingly spheroidal particles change their scattering behavior toward lower depolarization ratios. However, this argument is not conclusive. Scattering phase matrices are predominantly determined by reflections at crystal surfaces, and therefore sublimation-induced alteration of edge and corner radii may be better regarded as distortions of the initial particle habits, having relatively little effect on the scattering signature, specifically the depolarization ratio. Laboratory and theoretical studies seem to support this assumption. *Sassen* [1977] reported depolarization ratios between 52% and 59% for frozen rainwater drops with a regular spherical or spheroidal appearance. T-matrix calculations performed for spheroids, circular cylinders, and deformed spheroids (Chebyshev particles) by *Mishchenko and Sassen* [1998] show that these rounded crystals have depolarization ratios that are comparable with, or larger than, δ_{par} values of hexagonal plates obtained with the ray-tracing method. Although the size parameters of the particles assumed for the T-matrix calculations are smaller than those normally found in cirrus clouds, these theoretical results, just like the experimental findings, suggest that evaporation of the ice crystals does not have to be invoked for the explanation of the observed low depolarization ratios. Sublimation may be also ruled out as a major cause for the low-depolarization data subset for observational reasons. Simultaneously with the cirrus measurements, water vapor was measured with the GKSS Raman lidar. From the moisture data and from radiosonde temperature observations we retrieved estimates of relative humidity with respect to ice (Fig. 10). The low absolute humidity over Esrange resulted in weak water-vapor lidar signals that require long data integration times and restrict this analysis to altitudes < 6–7 km. This does not pose a major problem for the discussion here, because measurement segments with relatively stable lower cloud boundary could be chosen for the integration, and most of the low-δ_{par} cirrus data are found towards the bases of the clouds. A more serious limitation of the quality of the relative-humidity data that complicates its interpretation is that temperature was not observed together with the lidar measurements at the lidar site. Although caution has to be applied, the relative-humidity data indicate that in all cases the cirrus clouds developed in air layers which were most likely saturated or supersaturated with respect to ice (0–20% supersaturation) at cirrus altitudes where low particle depolarization is found. This conclusion is corroborated by the analysis of the cloud extinction profiles, as the extinction coefficient is usually at its maximum in the lower cirrus layers, indicating particle growth rather than evaporation. For these reasons, sublimation is not considered in our microphysical interpretation.

Figure 10. Relative humidity with respect to ice (RHI) retrieved from lidar water-vapor and radiosonde temperature data. Lidar data were integrated over measurement intervals for which the cirrus clouds extended to low altitudes (times corresponding to the centers of the intervals are indicated). Range of cloud base height during the water-vapor measurement intervals (shaded areas), and cloud base height as observed during the cirrus measurement segments with low δ_{par} (horizontal solid line) are given for comparison. Error bars indicate the standard deviation due to signal noise. Temperature profiles were taken from radiosondes measurements at the lidar site (8 January 1997, 14:00 UT), or at the radiosonde station Luleå (240 km south of Esrange; 17 and 20 January 1997, 00:00 UT).

6. Conclusions

We have shown in this study how the polarization Raman lidar data of cirrus clouds that evolved over the Swedish research facility in January 1997 can be interpreted in terms of the sizes and shapes of the scattering ice particles, and, under additional assumptions about the atmospheric conditions prevalent during the observations, in terms of growth, or more general, morphological development of the cirrus particles. It turned out that key to the understanding of light scattering by cirrus clouds is simultaneous measurement of particle depolarization ratios and lidar ratios. However, we would like to stress the obvious fact that, although the given interpretation appears plausible, it is by no means proven. Important issues remain to be resolved which include, among others, the relation between the optical and the microphysical properties of realistic ice particles, the influence of particle orientation, and the dynamic interpretation of the data. Furthermore, the question of the generality of our findings has to be addressed.

In order to improve the microphysical analysis of cirrus lidar data, more research, both experimental and theoretical, has to be conducted. Two especially helpful experiments would consist of concurrent lidar observations from the ground and airborne particle sampling, and simultaneous *in situ* measurements with microphysical instrumentation and a lidar analog. We have demonstrated that knowledge of supersaturation aids the interpretation of the cirrus

data. A shortcoming of our supersaturation data was that temperatures were not measured with the lidar, but had to be taken from radiosonde observations. Addition of cloud-temperature measurement capability to a lidar deployed in cirrus observations would be certainly desirable; the method that can be used for cloud temperature studies is the rotational Raman technique [*Behrendt and Reichardt*, 2000].

Also, improvements in calculation of optical properties of large crystals are necessary. The ray-by-ray-integration method appears to be well-suited for this task, since some of the restrictions that standard ray-tracing codes have do not apply here [*Yang and Liou*, 1997]. Finally, coupled optical and microphysical modeling might contribute to the understanding of the microphysical information content that is hidden in lidar measurements of cirrus clouds [*Reichardt et al.*, 2002a].

Acknowledgments. This work was funded by the European Commission (grant ENV4-CT95-0162), the German Bundesministerium für Bildung, Wissenschaft und Technologie (grant 01LO9504/5), and the NASA Radiation Sciences Program.

References

Ansmann, A., U. Wandinger, M. Riebesell, C. Weitkamp, and W. Michaelis, Independent measurement of extinction and backscatter profiles in cirrus clouds by using a combined Raman elastic-backscatter lidar, *Appl. Opt.*, *31*, 7113–7131, 1992.

Auer, A. H., Jr., and D. L. Veal, The dimension of ice crystals in natural clouds, *J. Atmos. Sci.*, *27*, 919–926, 1970.

Baker, M. B., Cloud microphysics and climate, *Science*, *276*, 1072–1078, 1997.

Behrendt, A., and J. Reichardt, Atmospheric temperature profiling in the presence of clouds with a pure rotational Raman lidar by use of an interference-filter-based polychromator, *Appl. Opt.*, *39*, 1372–1378, 2000.

Carslaw, K. S., M. Wirth, A. Tsias, B. P. Luo, A. Dörnbrack, M. Leutbecher, H. Volkert, W. Renger, J. T. Bacmeister, and T. Peter, Particle microphysics and chemistry in remotely observed mountain polar stratospheric clouds, *J. Geophys. Res.*, *103*, 5785–5796, 1998.

Del Guasta, M., M. Morandi, L. Stefanutti, J. Brechet, and J. Piquard, One year of cloud lidar data from Dumont d'Urville (Antarctica). I. General overview of geometrical and optical properties, *j. Geophys. Res.*, *98*, 18,575–18,587, 1993.

Del Guasta, M., M. Morandi, L. Stefanutti, B. Stein, and J. P. Wolf, Derivation of Mount Pinatubo stratospheric aerosol mean size distribution by means of a multiwavelength lidar, *Appl. Opt.*, *33*, 5690–5697, 1994.

Del Guasta, M., Simulation of LIDAR returns from pristine and deformed hexagonal ice prisms in cold cirrus by means of "face tracing", *J. Geophys. Res.*, *106*, 12,589–12,602, 2001.

Eloranta, E. W., and P. Piironen, Measurements of cirrus cloud optical properties and particle size with the University of Wisconsin High Spectral Resolution Lidar, in *Advances in Atmospheric Remote Sensing with Lidar*, edited by A. Ansmann, R. Neuber, P. Rairoux, and U. Wandinger, pp. 83–86, Springer, New York, 1997.

Eloranta, E. W., R. E. Kuehn, and R. E. Holz, Measurements of backscatter phase function and depolarization in cirrus clouds made with the University of Wisconsin High Spectral Resolution Lidar, in *Advances in Laser Remote Sensing*, edited by A. Dabas, C. Loth, and J. Pelon, pp. 255–257, Ecole Polytechnique, Paris, 2001.

Gonda, T., and T. Yamazaki, Morphology of ice droxtals grown from supercooled water droplets, *J. Cryst. Growth*, *45*, 66–69, 1978.

Hess, M., R. B. A. Koelemeijer, and P. Stammes, Scattering matrices of imperfect hexagonal ice crystals, *J. Quant. Spectrosc. Radiat. Transfer*, *60*, 301–308 , 1998.

Heymsfield, A. J., Laboratory and field observations of the growth of columnar and plate crystals from frozen droplets, *J. Atmos. Sci.*, *30*, 1650–1656, 1973.

Heymsfield, A. J., and J. Iaquinta, Cirrus crystal terminal velocities, *J. Atmos. Sci.*, *57*, 916–938, 2000.

Intrieri, J. M., G. L. Stephens, W. L. Eberhard, and T. Uttal, A method for determining cirrus cloud particle sizes using lidar and radar backscatter technique, *J. Appl. Meteor.*, *32*, 1074–1082, 1993.

Macke, A., Scattering of light by polyhedral ice crystals, *Appl. Opt.*, *32*, 2780–2788, 1993.

Mason, B. J., G. W. Bryant, and A. P. van den Heuvel, The growth habits and surface structure of ice crystals, *Phil. Mag.*, *8*, 505–526, 1963.

Mehrtens, H., U. von Zahn, F. Fierli, B. Nardi, and T. Deshler, Type I PSC-particle properties: Measurements at ALOMAR 1995 to 1997, *Geophys. Res. Lett.*, *26*, 603–606, 1999.

Mishchenko, M. I., and K. Sassen, Depolarization of lidar returns by small ice crystals: an application to contrails, *Geophys. Res. Lett.*, *25*, 309–312, 1998.

Müller, D., U. Wandinger, D. Althausen, I. Mattis, and A. Ansmann, Retrieval of physical particle properties from lidar observations of extinction and backscatter at multiple wavelengths, *Appl. Opt.*, *37*, 2260–2263, 1998.

Müller, D., U. Wandinger, D. Althausen, and M. Fiebig, Comprehensive particle characterization from three-wavelength Raman-lidar observations: Case study, *Appl. Opt.*, *40*, 4863–4869, 2001.

Nelson, J., Sublimation of ice crystals, *J. Atmos. Sci.*, *55*, 910–919, 1998.

Platt, C. M. R., Lidar backscatter from horizontal ice crystal plates, *J. Appl. Meteor.*, *17*, 482–488, 1978.

Platt, C. M. R., and A. C. Dilley, Remote sensing of high clouds. IV: Observed temperature variations in cirrus optical properties, *J. Atmos. Sci.*, *38*, 1069–1082, 1981.

Platt, C. M. R., N. L. Abshire, and G. T. McNice, Some microphysical properties of an ice cloud from lidar observation of horizontally oriented crystals, *J. Appl. Meteor.*, *17*, 1220–1224, 1978.

Pruppacher, H. R., and J. D. Klett, *Microphysics of Clouds and Precipitation* (Reidel, Dordrecht, 1980).

Reichardt, J., Optical and geometrical properties of northern midlatitude cirrus clouds observed with a UV Raman lidar, *Phys. Chem. Earth*, *24*, 255–260, 1999.

Reichardt, J., U. Wandinger, M. Serwazi, and C. Weitkamp, Combined Raman lidar for aerosol, ozone, and moisture measurements, *Opt. Eng.*, *35*, 1457–1465, 1996.

Reichardt, J., R.-F. Lin, S. Reichardt, T. J. McGee, and D. O'C. Starr, Microphysical interpretation of cirrus measurements with lidar – comparison to a coupled optical-microphysical model, American Meteorological Society's 11th Conference on Cloud Physics, Ogden, Utah, 2002a.

Reichardt, J., S. Reichardt, A. Behrendt, and T. J. McGee, Correlations among the optical properties of cirrus-cloud particles: Implications for spaceborne remote sensing, *Geophys. Res. Lett.*, accepted, 2002b.

Rosenfeld, D., and W. L. Woodley, Deep convective clouds with sustained supercooled liquid water down to $-37.5°C$, *Nature*, *405*, 440–442, 2000.

Sassen, K., Optical backscattering from near-spherical water, ice, and mixed phase drops, *Appl. Opt.*, *16*, 1332–1341, 1977.

Sassen, K., Remote sensing of planar ice crystal fall attitudes, *J. Meteor. Soc. Japan*, *58*, 422–429, 1980.

Sassen, K., The polarization lidar technique for cloud research: A review and current assessment, *Bull. Amer. Meteor. Soc.*, *72*, 1848–1866, 1991.

Sassen, K., Evidence for liquid-phase cirrus cloud formation from volcanic aerosols: Climatic implicatons, *Science*, *257*, 516–519, 1992.

Sassen, K., and Y. Takano, Parry arc: A polarization lidar, ray-tracing, and aircraft case study, *Appl. Opt.*, *39*, 6738–6745, 2000.

Sassen, K., and S. Benson, A midlatitude cirrus cloud climatology from the Facility for Atmospheric Remote Sensing. Part II: Microphysical properties derived from lidar depolarization, *J. Atmos. Sci.*, *58*, 2103–2112, 2001.

Sassen, K., and J. M. Comstock, A midlatitude cirrus cloud climatology from the Facility for Atmospheric Remote Sensing. Part III: Radiative properties, *J. Atmos. Sci.*, *58*, 2113–2127, 2001.

Sassen, K., K. N. Liou, S. Kinne, and M. Griffin, Highly supercooled cirrus cloud water: Confirmation and climatic implications, *Science*, *227*, 411–413, 1985.

Sassen, K., R. P. Benson, and J. D. Spinhirne, Tropical cirrus cloud properties derived from TOGA/COARE airborne polarization lidar, *Geophys. Res. Lett.*, *27*, 673–676, 2000.

Sassen, K., J. M. Comstock, Z. Wang, and G. C. Mace, Cloud and aerosol research capabilities at FARS: The Facility for Atmospheric Remote Sensing, *Bull. Amer. Meteor. Soc.*, *82*, 1119–1138, 2001.

Takano, Y., and K. N. Liou, Radiative transfer in cirrus clouds. Part III: Light scattering by irregular ice crystals, *J. Atmos. Sci.*, *52*, 818–837, 1995.

Wandinger, U., A. Ansmann, J. Reichardt, and T. Deshler, Determination of stratospheric aerosol microphysical properties from independent extinction and backscattering measurements with a Raman lidar, *Appl. Opt.*, *34*, 8315–8329, 1995.

Wettlaufer, J. S., Impurity effects in the premelting of ice, *Phys. Rev. Lett.*, *82*, 2516–2519, 1999.

Yang, P., and K. N. Liou, Light scattering by hexagonal ice crystals: Solutions by a ray-by-ray integration algorithm, *J. Opt. Soc. Am. A*, *14*, 2278–2289, 1997.

Yang, P., and K. N. Liou, Single-scattering properties of complex ice crystals in terrestrial atmosphere, *Contr. Atmos. Phys.*, *71*, 223–248, 1998.

Yang, P., B.-C. Gao, B. A. Baum, W. J. Wiscombe, Y. X. Hu, S. L. Nasiri, P. F. Soulen, A. J. Heymsfield, G. M. McFarquhar, and L. M. Miloshevich, Sensitivity of cirrus bidirectional reflectance to vertical inhomogeneity of ice crystal habits and size distributions for two Moderate-Resolution Imaging Spectroradiometer (MODIS) bands, *J. Geophys. Res.*, *106*, 17,267-17,291, 2001.

J. Reichardt, Atmospheric Chemistry and Dynamics Branch, Laboratory for Atmospheres, NASA Goddard Space Flight Center, Greenbelt, MD 20771, USA. (reichardt@code916.gsfc.nasa.gov)

S. Reichardt, Atmospheric Chemistry and Dynamics Branch, Laboratory for Atmospheres, NASA Goddard Space Flight Center, Greenbelt, MD 20771, USA. (sreichardt@aeolus.gsfc.nasa.gov)

M. Hess, Remote Sensing Technology Institute, DLR - German Aerospace Center, Oberpfaffenhofen, D-82234 Weßling, Germany. (michael.hess@dlr.de)

T. J. McGee, Atmospheric Chemistry and Dynamics Branch, Laboratory for Atmospheres, NASA Goddard Space Flight Center, Greenbelt, MD 20771, USA. (mcgee@aeolus.gsfc.nasa.gov)

(Received _____.)

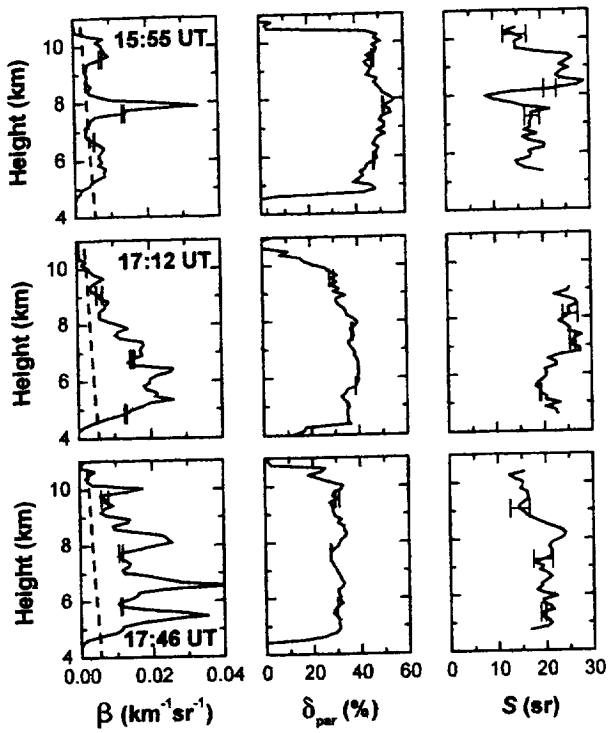

Fig. 1

J. Reichardt
J. Geophys. Res.

Bilder
Journal-Version
JGR2002

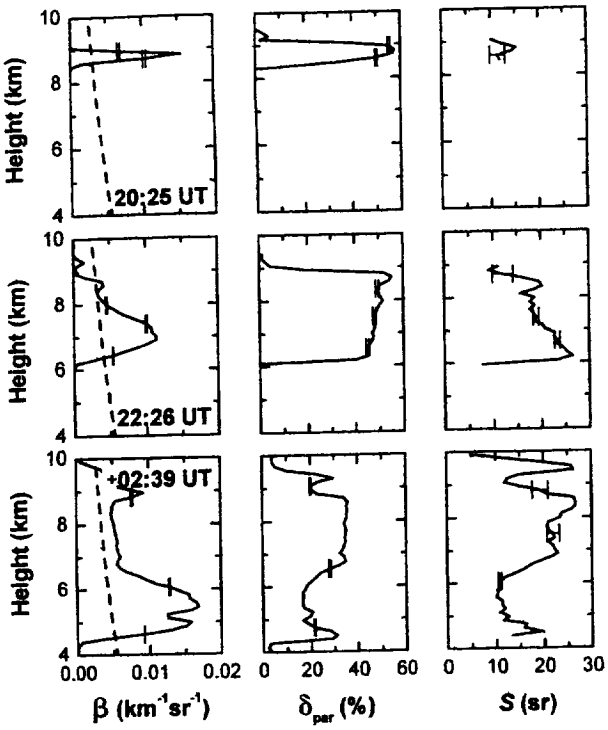

Fig. 2

J. Reichardt
J. Geophys. Res.

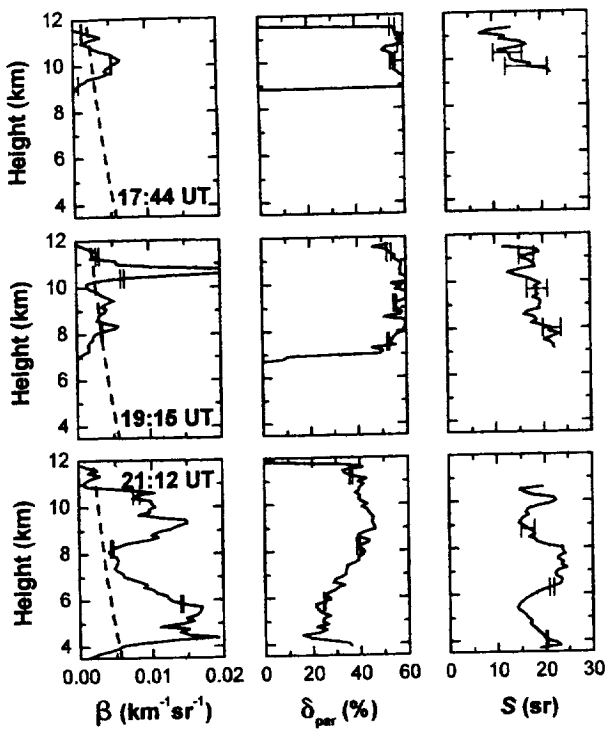

Fig. 3

J. Reichardt

J. Geophys. Res.

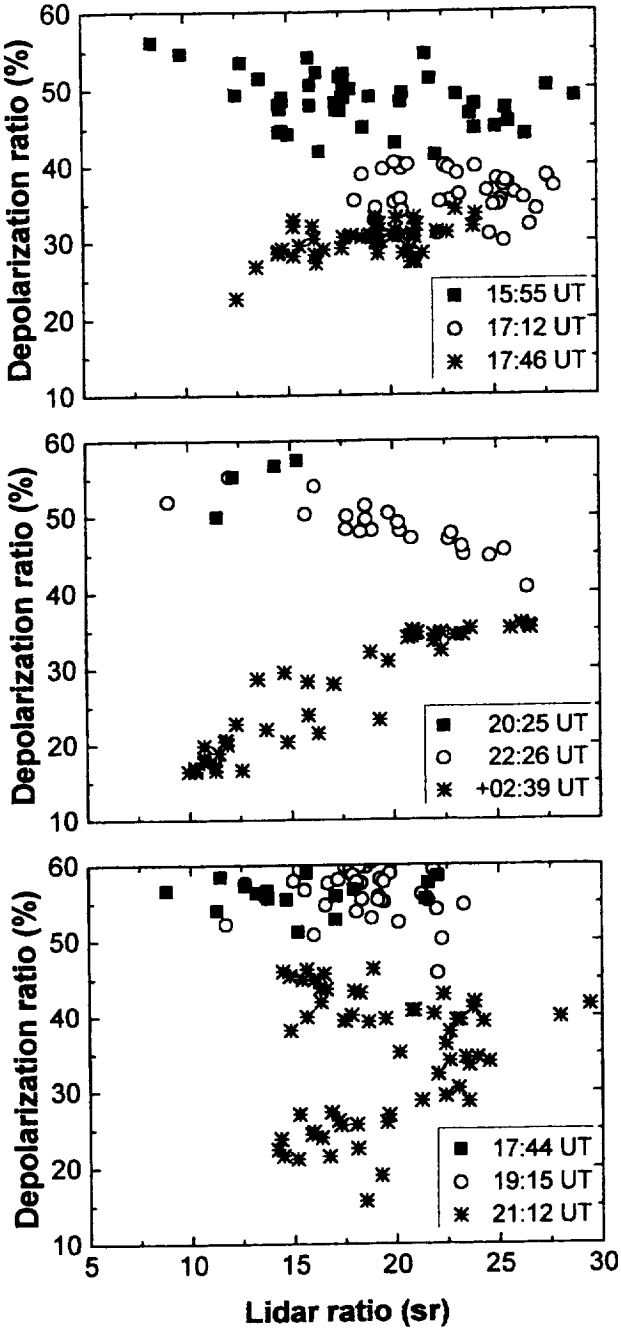

Fig. 4

J. Reichardt
Geophys. Res. Lett.

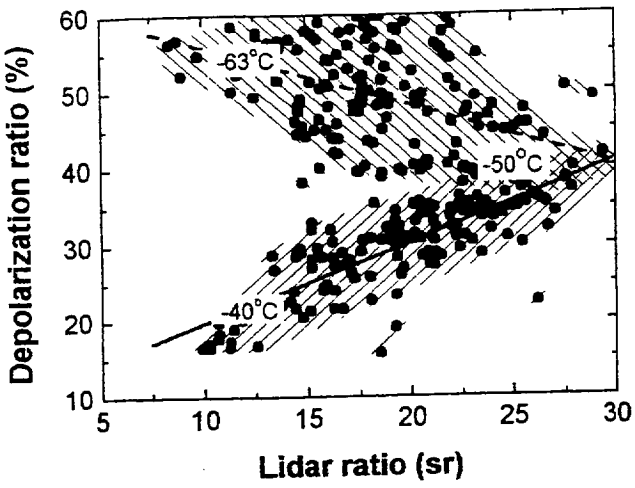

Fig. 5

J. Reichardt
J. Geophys. Res.

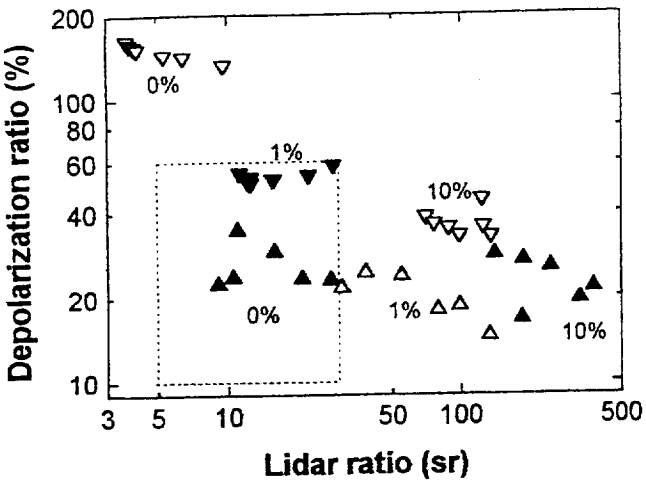

Fig. 6

J. Reichardt
J. Geophys. Res.

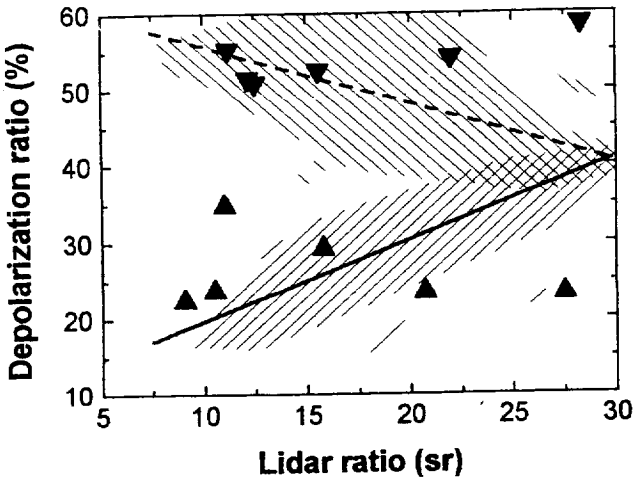

Fig. 7

J. Reichardt
J. Geophys. Res.

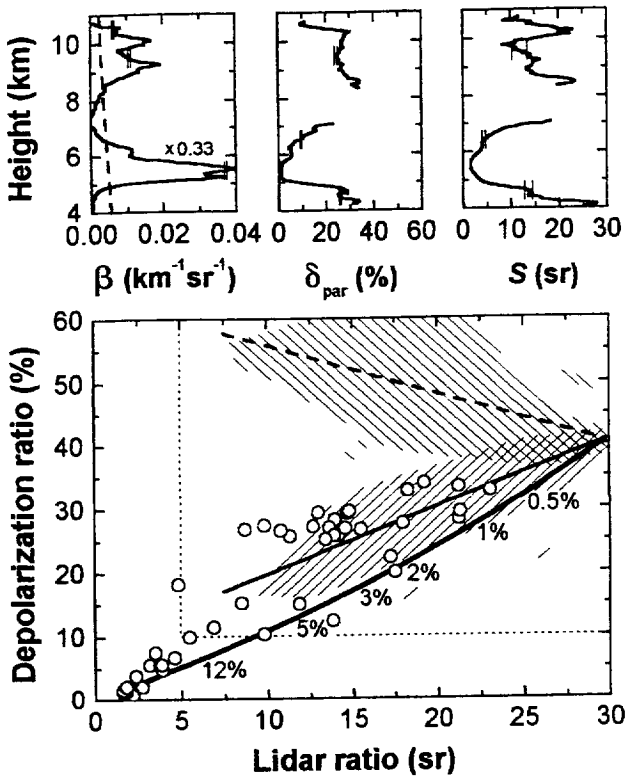

Fig. 8

J. Reichardt
J. Geophys. Res.

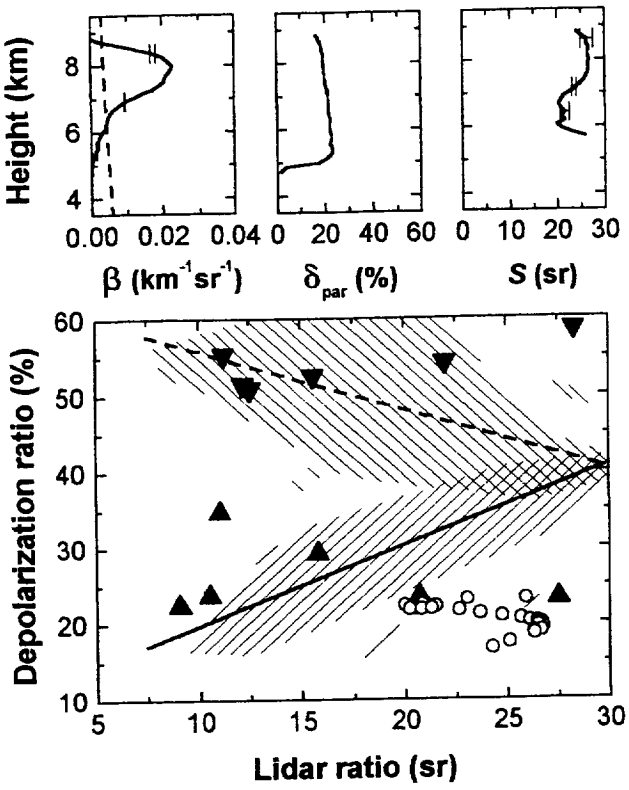

Fig. 9

J. Reichardt
J. Geophys. Res.

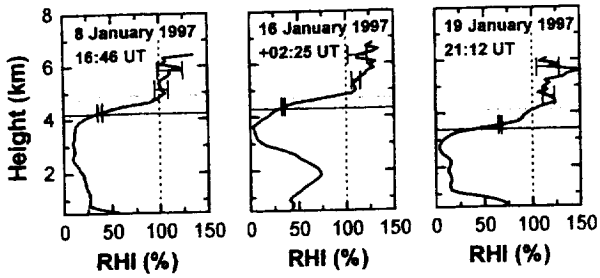

Fig. 10

J. Reichardt
J. Geophys. Res.